Journal of Power Sources 193 (2009) 241–248

Contents lists available at ScienceDirect

Journal of Power Sources

journal homepage: www.elsevier.com/locate/jpowsour

The effect of temperature gradients on thermal cycling and isothermal ageing of micro-tubular solid oxide fuel cells

C.M. Dikwal*, W. Bujalski, K. Kendall

Department of Chemical Engineering, University of Birmingham, Birmingham, West Midlands B15 2TT, United Kingdom

ARTICLE INFO

Article history:
Received 2 October 2008
Received in revised form 30 December 2008
Accepted 19 January 2009
Available online 10 February 2009

Keywords:
SOFC
Cycling
Thermal
Degradation
Temperature
Micro-tubular

ABSTRACT

Isothermal ageing and thermal cycling are performed on micro-tubular solid oxide fuel cells (SOFCs) in-order to understand degradation and failure mechanisms in micro-tubular SOFCs. For isothermal ageing, the effect of temperature gradients is investigated at 800 °C on two micro-tubular SOFC samples (1) 25 mm long and (2) 55 mm long. A temperature gradient is induced across the cells by passing 25% excess fuel for combustion at the cell outlet, thereby raising the temperature at this end to 950 °C. 25 mm long samples presented higher power density than the later ones and their rates of degradation were similar. Also, the effect of temperature gradients is investigated during the thermal cycling of micro-tubular SOFC to understand their contribution to electrochemical performance degradation. Two micro-tubes were characterized; one with optimum hydrogen flow rate and the other with 25% excess. No micro-cracking or de-lamination was observed in the micro-tube without a temperature gradient, whereas severe de-laminations and micro-cracking were observed when 25% excess hydrogen flow was used during thermal cycling.

In conclusion, the effect of temperature gradients during isothermal ageing was marginal, and Ni sintering was found to dominate the degradation mechanism. On the other hand during thermal cycling, the temperature gradients were found to be contributive to degradation by opening micro-cracks and de-laminations.

1. Introduction

Reliability and durability are important parameters in SOFC design and commercialization; as such studies into factors that undermine them such as thermal stresses is important. The recent commercial requirement of SOFC is a working lifetime of 40,000–50,000 h (during which they would undergo several thermal cycles as thermal cycling is inevitable during SOFC operation). Thermal cycling has been identified as one of the main factors responsible for stress induction and performance degradation in SOFC, the degradation occurring principally in the Membrane-Electrode-Assembly (MEA) due to stress build up, fatigue and thermal shock [1]. Properties of ceramics such as high melting point and thermal shock resistance make them useful in thermal applications such as high temperature fuel cell [2,3]. Thermal shock resistance is an index that relates both the thermal properties and mechanical properties of a ceramic. It is the ability of a material to withstand rapid and immediate temperature changes at given time intervals without failure. Thermal shock arises when there is a sudden change in temperature in a ceramic, causing mechanical changes and fracture in the bulk of the material. In addition to thermal shock, temperature gradients are likely to occur in SOFC because of the electrochemical reactions which occur in the cell coupled with the non-uniform heat distributions [4].

Thermal cycling is inevitable in solid oxide fuel cells (SOFCs) as they are started, and shutdown periodically [5–8]. The main effect of thermal cycling on composite materials is thermal stress induction which arises from coefficient of thermal expansion mismatch between the different components that make up the SOFC. To better understand the effect of expansion mismatch between the various components, the fabrication processes of the fuel cell should be considered from co-extrusion to sintering and cooling. Stress starts to build up during the fabrication stage as the powder-binder slurry of NiO/YSZ transforms into a dense ceramic, as a result of the volume change that could occur during this transformation. Cracking can occur at this stage under inappropriate conditions [9].

Also, residual stresses build up after fabrication as the fuel cell is cooled from sintering temperature to room temperature, mainly because of the intimate contact between the metal and ceramic phases which contract by different indexes. At the sintering temperature, all the cell components are at thermal equilibrium; this is made possible by the adherence of the components at this temperature. During cooling, the adhered particles shrink inducing contractive stresses. Even greater stresses are known to be

* Corresponding author. Tel.: +44 0 1214145276; fax: +44 0 1214145324.
E-mail address: chinnand@yahoo.com (C.M. Dikwal).

0378-7753/$ – see front matter © 2009 Elsevier B.V. All rights reserved.
doi:10.1016/j.jpowsour.2009.01.097

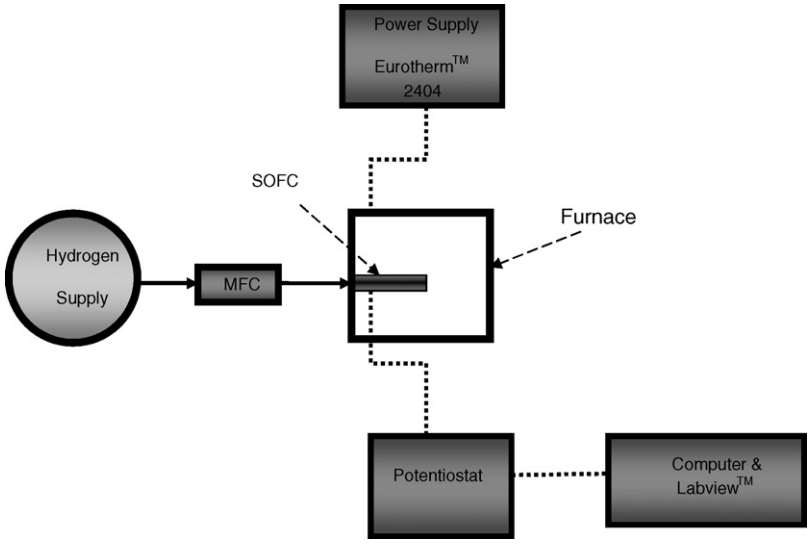

Fig. 1. The schematic for the cycling setup.

induced in SOFC during operation; the main culprits of stress induction during SOFC operation include fatigue, thermal shock, thermally induced stress, residual stress levels [10,11]. Thermally induced stresses arise due to the existence of temperature gradients within a homogenous material. If two points within a material are at different temperatures, they would expand by different indexes thereby causing a state of tension between the two points; this could lead to stress induction or possible failure. Additionally, stress also builds up during the reduction stage, where the NiO/YSZ anode is transformed to Ni/YSZ cermets by stripping off the oxygen ion using a reducing atmosphere (usually hydrogen). The oxygen ions removed causes the Ni particles shrink, but the shrinkage is constrained by the dense ceramic leading to further stress induction.

2. Experimental method

Most thermal cycling studies of SOFC have focused on planar SOFC [12,13], with very little attention to the cycling performance of micro-tubular SOFC. A large number of the thermal stress models developed are based on the inherent residual stresses and the thermal stresses induced during operation. Bujalski et al. [14] have performed 100 thermal cycles on integrated planar Rolls Royce Fuel Cell system (RRFCS) integrated planar (IP) tubes showing slight degradation. The objective of this study is to investigate the effect of temperature gradients across micro-tubular SOFCs under isothermal ageing and thermal cycling conditions.

2.1. Sample preparation

Two different lengths of micro-tubular SOFC samples were characterized for the isothermal ageing experiments; (1) 25 mm long (hereinafter referred to as short cells) (2) 55 mm long (hereinafter referred to as long cells), the reason for characterizing two different sample lengths was to investigate the effect of temperature gradients on the size of the micro-tubes during constant temperature operation. For the thermal cycling experiment, only the 55 mm long micro-tubes were tested.

The Raw micro-tubes (anode-electrolyte) were co-extruded and supplied by Adaptive Materials Incorporated (AMI), USA. The cells were supplied already sintered with an anode thickness of 200 μm and 15 μm of electrolyte. Cathode formulation and preparation are as detailed in [15], the cathode layers were added-on by hand painting. Two cathode layers were painted, the first layer was 50% Yttria stabilized Zirconia (YSZ) and 50% lanthanum Strontium manganate (LSM). The YSZ layer in the cathode is essential to adhere the cathode layer to the YSZ electrolyte. The second layer consisted of 15% YSZ and 85% LSM, the reason for the variation in composition is for the purpose of adhering similar components together in-order to minimize de-laminations or cracking due to expansion mis-match. After the addition of both cathode layers with sufficient drying time, the samples are heated to 500 °C at 1 °C min^{-1} in order to burn-out the pore former followed by heating to 1150 °C at 12.5 °C min^{-1} and sintering at this temperature for 2 h before cooling down to room temperature at 20 °C min^{-1}. The cathode active area was 1.57 cm^2 for the long cells and 1.256 cm^2 for the short cells. Silver paint and silver wire were used to collect the current from the cathode while the electrolyte surface was polished-off to expose the anode for collection of current.

2.2. Thermal cycling experiment

Thermal cycling was performed only on the long cells; the rig comprised a Eurotherm™ 2404 power controller attached to a brick furnace. The fuel cell was located in the furnace centre, supported by a fuel injecting manifold which carried the fuel. The fuel

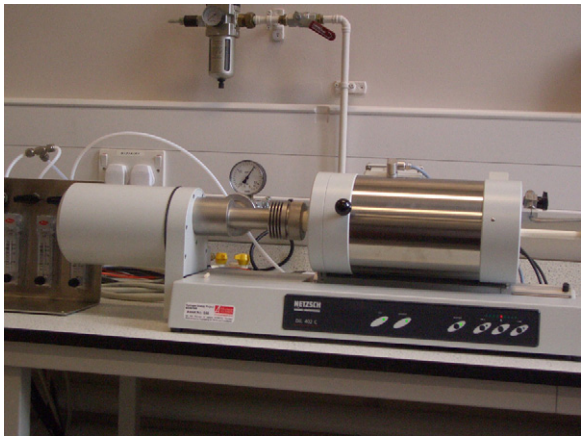

Fig. 2. The dilatometry system used in the study.

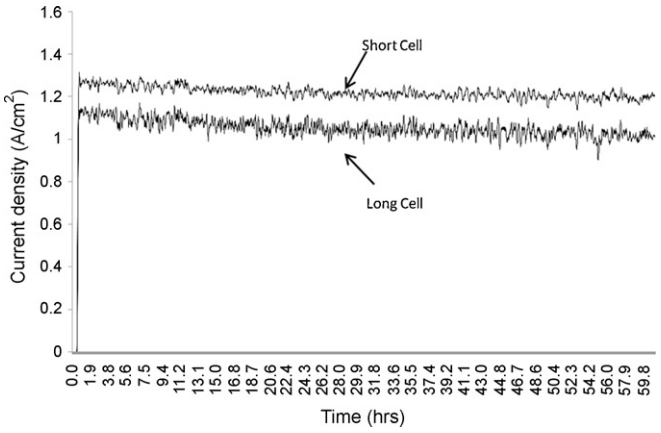

Fig. 3. Isothermal ageing of a 25 mm cell and a 55 mm cell, respectively.

(hydrogen) flow was set by a mass flow controller attached to a gas cylinder. The oxygen required by the air-electrode was obtained from atmospheric air (being that the furnace had a few large holes). Voltage and current measurements were carried-out using a potentiostat interfaced with a Labview™ software. Fig. 1 is a schematic of the cycling setup. Prior to the cycling experiment, the micro-tubular SOFC was reduced in 10 ml min^{-1} of hydrogen at 750 °C for 45 min in order to convert the NiO/YSZ anode to an Ni/YSZ cermet.

The objective of the experiment is to evaluate effects of thermal gradients on the thermal cycling behaviour of micro-tubular SOFCs. To do this, two long cells were tested, one with 25% excess hydrogen flow and the other with optimum hydrogen flow (20 ml min^{-1}). The excess fuel was necessary in order to cause combustion at the fuel outlet so as to raise the temperature at this end, thereby creating a temperature gradient across the tube while the cell was being cycled thermally. The same temperature profile was used during thermal cycling for both cells. For both cells, the open circuit voltage was measured at 1.08 V then current was drawn at 0.5 V. The first segment of thermal cycling proceeded by ramping the furnace to 800 °C at 200 °C min^{-1}, the second segment was the constant temperature hold for 3 min at 800 °C. The third segment was cooling down to 200 °C at 120 °C min^{-1}; a large portion of this segment is dependent on natural convection to the atmosphere. The final segment was a constant temperature hold at 200 °C for 5 min, necessary to equilibrate the SOFC. The cells were held under load (0.5 V) all through the experiment.

2.3. Isothermal ageing experiment

Short and long micro-tubes were characterized and tested under isothermal conditions. The objective was to investigate the effect of temperature gradients and the size-effect of micro-tubes. The micro-tubular SOFCs were operated in the same test rig as for the thermal cycling. The fuel cells was ramped up to 800 °C at 200 °C min^{-1} in 25% excess hydrogen and the open circuit voltage was measured. Subsequently, the current was drawn at 0.5 V and held for 60 h at 800 °C. The excess fuel was necessary for combustion at the cell outlet, so as to raise the temperature at this end and create a temperature differential across the tube.

2.4. Dilatometry experiment

The dilatometry system (Netzsch™ Dil 402C), Fig. 2, comprised a silicon carbide furnace, alumina protective tubes and sample holder. Temperature measurements at the sample were achieved using an S-type thermocouple, and the system was calibrated using alumina standards prior to measurement. The system was evacuated and back-filled with nitrogen prior to commencing the experiments. In the first thermal cycling experiment, the sample was heated to 800 °C at 10 °C min^{-1} in nitrogen, a thermal expansion coefficient of 1.25×10^{-6} °C^{-1} was estimated, and then the sample was held at 800 °C for 30 min and subsequently cooled down to 200 °C at 5 °C min^{-1}, the final segment which was a constant temperature hold at 200 °C for 30 min, a total of 9 thermal cycles were performed. In the second thermal cycling experiment, the sample was heated to 800 °C at 10 °C min^{-1} in nitrogen; it was held for 10 min at 800 °C then cooled down at 10 °C min^{-1} to 200 °C and holding for 10 min. 22 thermal cycles were achieved using this profile.

3. Results and discussion

3.1. Effect of temperature gradients on the isothermal ageing of 25 mm and 55 mm long micro-tubular SOFC

To investigate the effect of temperature gradients on the micro-tubes during isothermal operation, two types of micro-tubes were characterized; 55 mm long tubes (hereinafter referred to as long cells) and 25 mm long micro-tubes (hereinafter referred to as short cells). The objective was to investigate the effect of a temperature gradient on the micro-tubes with respect to their sizes. The cells were both operated in 25% excess hydrogen flow at 800 °C. The excess fuel flow was necessary so as to cause combustion at the

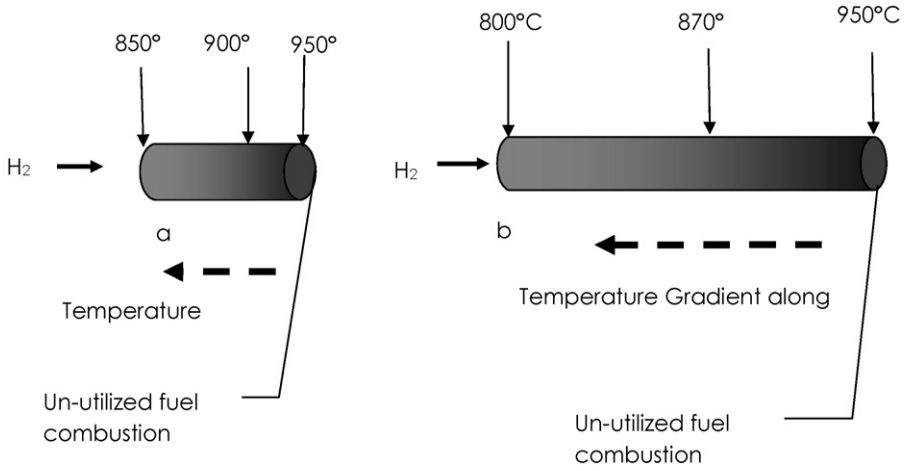

Fig. 4. Temperature gradients along the length of a micro-tubular SOFC.

fuel outlet and raise the temperature of this end, thus creating a temperature gradient along the tube.

As shown in Fig. 3, the short cells presented higher current density than the long tubes. This is primarily because the high ohmic resistance across the long cell due to longer electron paths in which the electrons produced had to travel to arrive at the current point. The current density of the short cells started at 1.30 A cm^{-2} and gradually decreased with time. The final current density after 60 h was 1.20 A cm^{-2}, which is slightly lower than the onset, giving a degradation rate of 0.81% h^{-1}. The 55 mm cell on the other hand showed a slightly lower current density, starting at 0.90 A cm^{-2} and gradually decreasing to 0.79 A cm^{-2}, giving degradation rate of 0.84% h^{-1}. For both samples the trend of degradation is similar. The first 20 h show a decrease in performance which is attributed to Ni particle agglomeration. Ni agglomeration will cause a change in the microstructure of the cells by decreasing the triple phase boundary layer necessary for fuel oxidation. The trend of degradation for both the short and long micro-tubes is similar to those reported in earlier studies by Dhir and Kendall [16] where the cells were operated in isothermal conditions. In that study, it was reported that sintering of the Ni anode dominated the first few hours of operation, accounting for most of the initial degradation before degradation due to ageing of the electrodes set in. Subsequent studies will be looking at the critical gradient necessary to cause fracture and micro-cracking in these micro-tubes, this is very important because in real life conditions an excess or incomplete utilization of fuel can impose a gradient along the tube causing fracture damage. Also, thermal shock is a likely occurrence in micro-tubular SOFCs due to their rapid start-up but in this study the effect of thermal shock is ignored because these micro-tubes have been found to withstand thermal shock [17].

Fig. 4 illustrates the temperature gradient along the tubes; the short micro-tube is found to heat up quicker and attains thermal equilibrium faster than the long micro-tube. The combustion of the excess fuel at the outlet raised the temperature of the end, thus creating a temperature differential along the tube. A lazer temperature probe and K-type thermo-couples were used to measure the temperature gradient.

At the combustion point, the temperature of the cell is 950 °C; this temperature decreases as you move along the tube. For the short micro-tubular SOFC, the difference between the inlet and outlet temperatures is smaller compared to the long micro-tube. The reason being the difference in heat transfer volume in the two samples.

The thermal gradient across the long cell was 150 °C. This caused the cell outlet (the combustion end) to expand by a larger index than the other end, causing stress induction. In severe conditions micro-cracking can occur especially where the magnitude of the gradient is large. The short micro-tube on the other hand had a smaller gradient (100 °C), thus its expansion differential was less. In

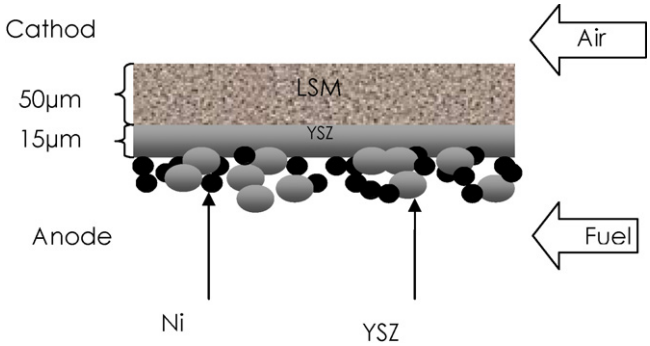

Fig. 5. The schematic of a micro-tube before sintering.

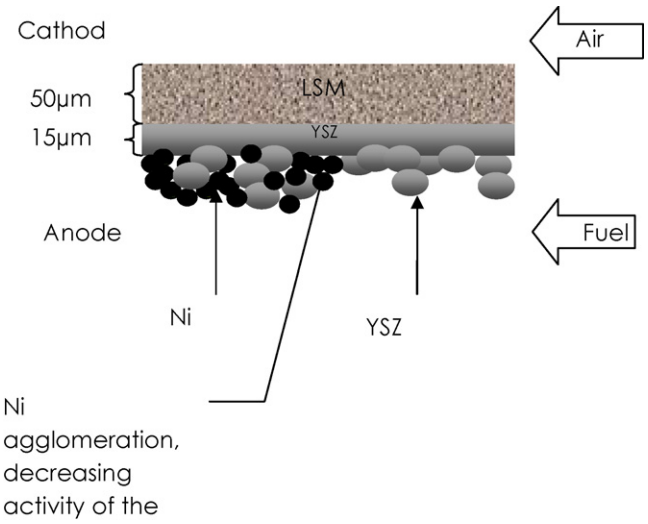

Fig. 6. A schematic of a micro-tube after sintering.

both cases, no micro-cracking was observed in the microstructure, thus it can be inferred that the temperature gradient imposed only had a contributive effect to stress accumulation in the bulk of the cells, but did not cause gross micro-cracking.

3.2. Sintering of the NI/YSZ anode

The main factor of electrochemical performance degradation in the micro-tubes was identified as sintering (agglomeration) of the Ni particles at high temperature. From Fig. 3, it can be seen that the first 20 h of operation showed a slight decrease in current density, this decrease in performance is attributed to the Ni agglomeration. Ni particles are extremely mobile at high temperature, causing them to agglomerate (sinter) [16]. The isothermal operation of the micro-tubes caused greater degree of sintering than thermal cycling because during isothermal operation, the cell was continuously held at high temperature (in the sintering regime) whereas during cycling the temperature goes up and down (in and out of the sintering regime).

Sintering causes the Ni particles to pull away from the YSZ particles thus inducing stress in the matrix. The final result of sintering is a dense agglomerated Ni substrate with decreased surface area. Ni sintering decreases the triple phase boundary layer necessary for electrochemical oxidation of fuel. A decrease in the triple phase boundary layer will translate to a decrease in electrochemical performance. Ceria based anodes and electrolytes are not limited by

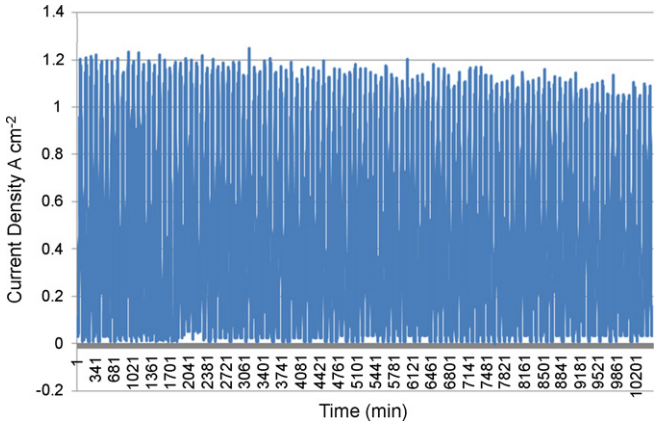

Fig. 7. Thermal cycling of a micro-tubular SOFC in optimum hydrogen flow.

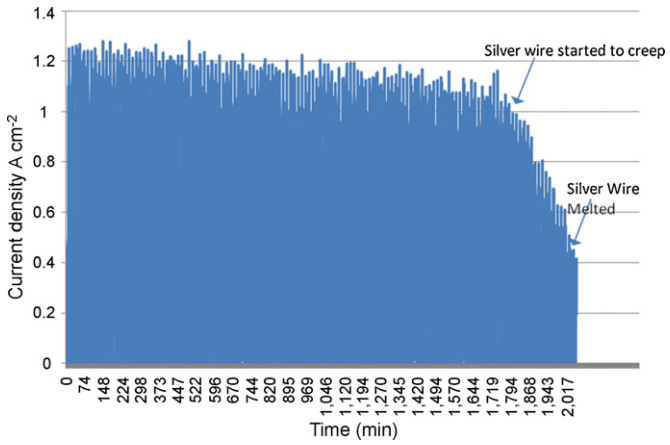

Fig. 8. Thermal cycling of a micro-tubular SOFC in 25% excess hydrogen flow.

this problem because the fuel oxidation occurs across the whole electrode and not necessarily at the triple phase boundary layer alone [18] Figs. 5 and 6 are schematic diagrams explaining this phenomenon. In Fig. 5 the schematic of an un-sintered micro-tube is presented, showing the uniform distribution of the Ni particles in the Ni/YSZ matrix before sintering. Subsequently, Fig. 6 shows the schematic of a sintered cell, where the Ni particles have agglomerated into a dense structure.

3.3. Thermal cycling results

Figs. 7 and 8 show the effects of thermal cycling between 200 °C and 800 °C on long micro-tubular SOFC cycled in hydrogen. In Fig. 7, the cell was cycled in 20 ml min^{-1} (i.e. optimum) of hydrogen while in Fig. 8, 25% excess hydrogen flow was used. The open circuit voltage (OCV) before thermal cycling in both cases was 1.08 V. At the commencement of cycling, only a slight decrease in current density is observed over several cycles unlike during isothermal ageing where the degradation is more significant. This slight degradation is principally because the rapid and continuous thermal cycling between high and low temperature did not allow for sufficient time at high temperature for sintering to occur. Dhir et al. have adduced sintering to be largely responsible for most of the initial degradation in Ni/YSZ anodes when operated isothermally at high temperatures [16]. In Fig. 7, an initial power density of 0.6 W cm^{-2} is observed before the commencement of thermal cycling, this drops to 0.54 W cm^{-2} after 110 thermal cycles. A degradation rate of 5.4×10^{-4} W $cycle^{-1}$ was evaluated. The optimum hydrogen flow ensured complete utilization of the fuel, thus no combustion occurred at the outlet of the cell. The degradation is therefore mainly due to the intrinsic material properties and cycling conditions. In Fig. 8, a power density of 0.64 W cm^{-2} is observed before the commencement of cycling, this decreases to 0.53 W cm^{-2} after 110 thermal cycles. A degradation rate of 1×10^{-3} W $cycle^{-1}$ is evaluated in this case. After the 118th thermal cycle, a rapid increase in the rate of degradation is observed as the silver interconnecting structure for the anode started to creep and melt, a degradation rate of 0.055 W $cycle^{-1}$ is evaluated during this period.

Table 1
The decrease in power density with cycling number.

Number of thermal cycles	Maximum power density (W cm^{-2})	Open circuit voltage OCV (V)
0	0.45	1.11
30	0.43	1.11
60	0.41	1.10
90	0.40	1.08
110	0.39	1.08

From Fig. 7 it can be argued that as cycling proceeded, severe thermal stresses are induced in the bulk of the cell due to cyclic expansion and contraction. The effect of thermal cycling is most severe at the material interfaces since each layer is composed of a different material [19]. Each component, i.e anode, cathode and electrolyte expands relative to its coefficient of thermal expansion (CTE), inducing expansive and contractive stresses between layers. With further cycling, stress continues to build up until it reaches a critical value where it has sufficient energy to drive micro-cracks and cause delamination in these material interfaces. In this case however, no micro-cracking or delamination was observed by SEM.

On the otherhand, the cell which had the temperature gradient imposed across it (i.e. Fig. 8) behaved in a different manner.

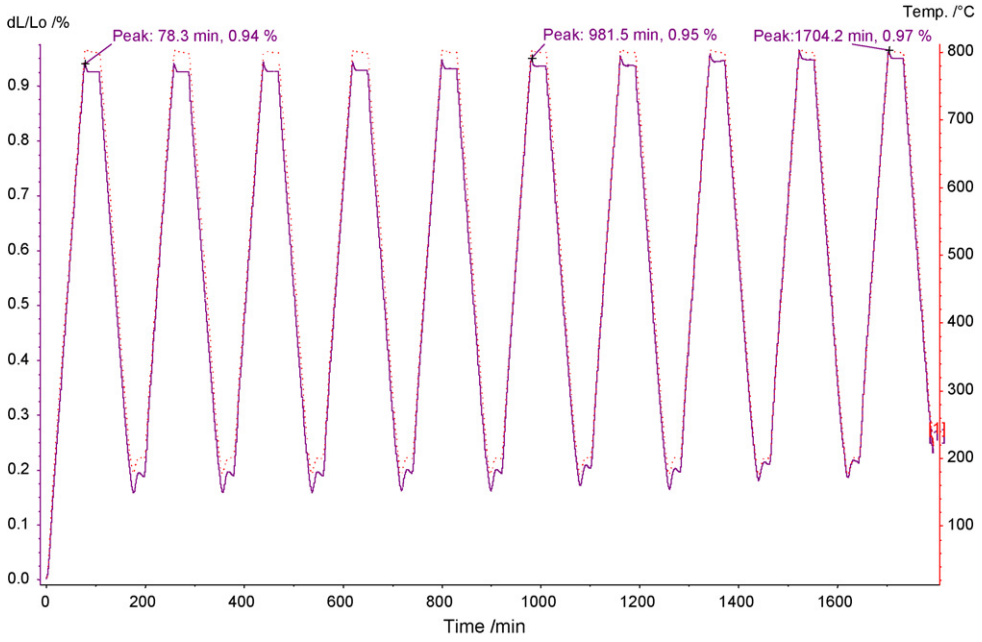

Fig. 9. The expansion and contraction of an SOFC by dilatometry during cycling.

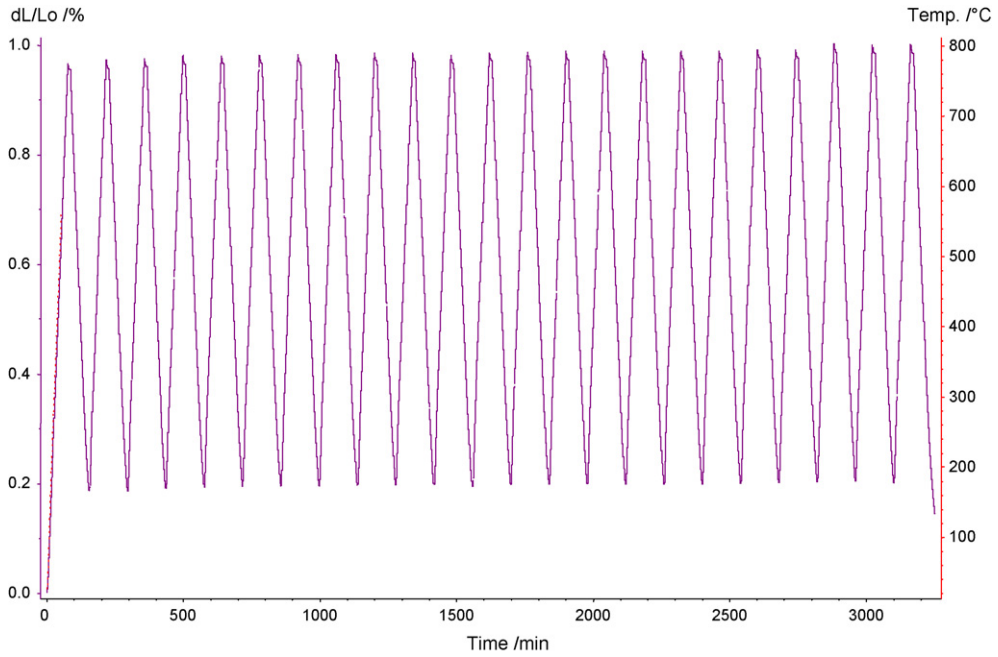

Fig. 10. The expansion and contraction under rapid and continuous thermal cycling.

It degraded by a larger index than compared to the one without a temperature gradient because of certain factors. During thermal cycling, the expansive and contractive forces were driven in all directions; radially (due to the CTE of the components) and length-wise (due to the temperature differential across the tube ends). Thus, if a crack opened-up due to radial expansion and contraction, it would be driven further by the length-wise expansion, this is because at the combustion end, the micro-tube expanded more than at the fuel inlet end, creating an expansion differential across the tube.

Expansion along the radius induced severe stresses mainly because of the contraint imposed by the other cell component which are in contact, causing delaminations. Delaminations are common occurences to relieve stresses when there are contraints or mismatch between the CTE of the components. The melting of the silver interconnecting structure as reported in Fig. 8, brings to light one of the problems associated with of SOFC interconnects [20,21]. SOFC interconnects such as silver, platinum etc are prone to stress induction during thermal cycling due to fatique and creep at high working temperature, making them prone to failure.

Table 1. shows the decrease in power density of a micro-tubular SOFC after several thermal cycles. Initially an open circuit voltage (OCV) of 1.08 V was observed before cycling, this is in agreement with the theoretical OCV for these conditions.

The power density is seen to decrease steadily as cycling proceeds, after 60 thermal cycles the power density is seen to decrease by 0.04 W cm^{-2} and by 0.06 W cm^{-2} after 110 thermal cycles. The

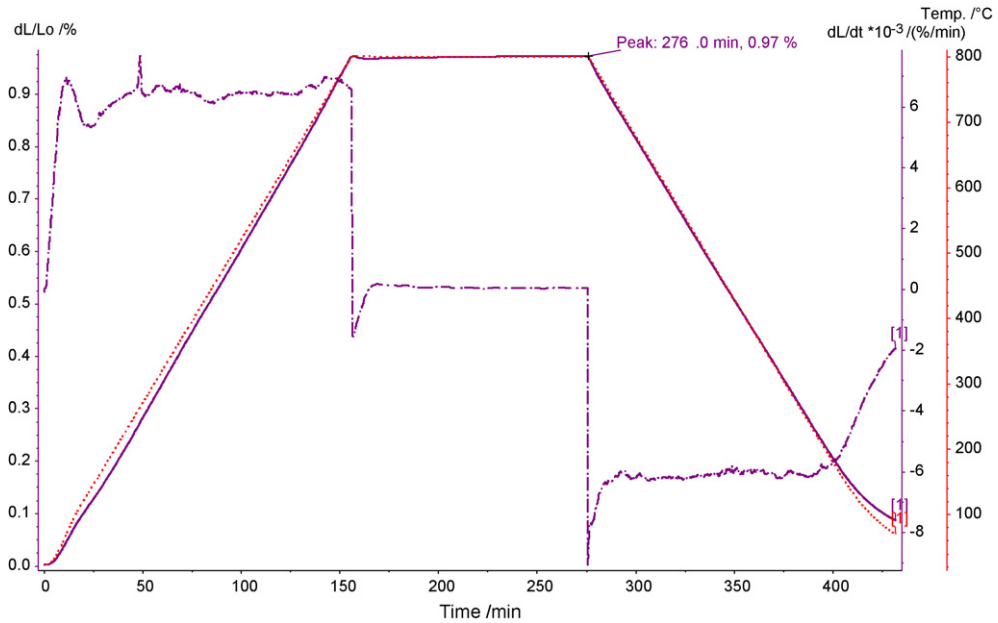

Fig. 11. The irreversible deformation of a sample due to sintering.

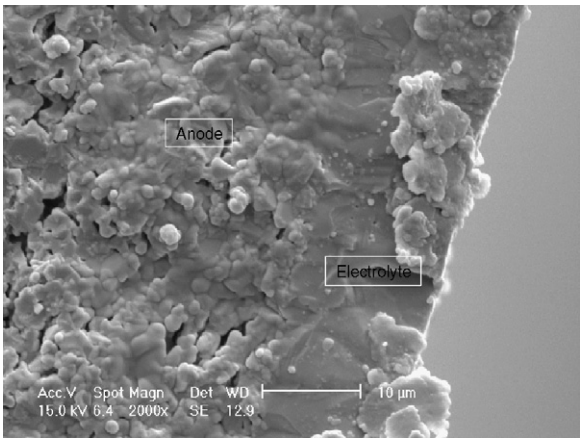

Fig. 12. A micrograph of an unreduced micro-tubular SOFC, showing the anode and electrolyte.

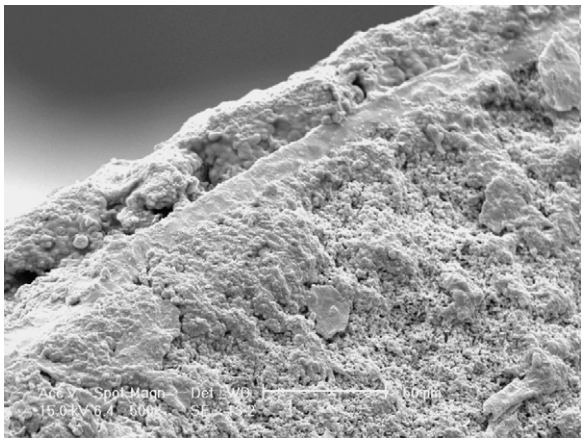

Fig. 14. A micrograph of a micro-tubular SOFC after cycling in optimum hydrogen flow.

initial trend of degradation during thermal cycling is similar to constant-temperature-hold experiments where no cycling is performed, the degradation mechanism being the sintering of the Ni anode which leads to a decrease in electro-active area necessary for fuel oxidation.

The effect of sintering on the micro-tubes has been shown to be more severe than the actual effect of the thermal cycling itself. From Fig. 7 sintering is seen to dominate the degradation mechanism throughout the experiment, as the electrochemical performance decreased steadily without any material delamination or micro-cracking, while in Fig. 8, a cummulative effect of sintering, together with the imposed temperature gradient and thermal cycling gave a more rapid degradation which even led to interconnect failure. Ni particle agglomeration can be minimized by depositing minute amounts of carbon or other elements in the microstructure to diminish this effect [15].

3.4. Dilatometry results

To show the extent of sintering occurring in the micro-tubes, dilatometry was performed. A temperature profile similar to that used for thermal cycling was used, where the cells were cycled between 200 °C and 800 °C in an inert atmosphere. In Fig. 9, the cell was cycled between 200 °C and 800 °C with a dwell time of 30 min at both temperatures, while in Fig. 10, a shorter dwell time of 10 min was used. Even though a longer dwell time was used in Fig. 9 where 9 thermal cycles were performed, the response of the sample was similar to Fig. 10 where a shorter well time was used; implying that the rapid cycling rate did not have much of an effect on the sample response. From Fig. 9, at 800 °C an expansion of 0.94% is observed against 0.205% at 200 °C. A thermal expansion coefficient of $12.5 \times 10^{-6}\,°C^{-1}$ was calculated for the bulk sample. A similar thermal expansion coefficient was evaluated in Fig. 10. However in this figure, it is seen that as cycling progresses there is irreversible deformation in the sample because the sample fails to recover back to its original length. Prior to cycling an expansion of 0.97% is observed, against 1.00% after 22 thermal cycles. This dimensional change in the cells is largely because of the sintering of Ni particles at high temperature causing irreversible movement. Once sintering occurs, the micro-structure of the anode changes due to the agglomeration of the Ni particles. This Ni agglomeration causes severe expansion because Ni has a higher thermal expansion coefficient than YSZ. With the commencement of the cooling segment, sintering becomes diminished as the sample is cooled to lower temperatures, however the micro-structural changes due to sintering are not reversed and once the next thermal cycle commences, further sintering and micro-structural changes proceed, leading to further dimensional change.

To clearly observe this irreversible deformation one thermal cycle is considered, see Fig. 11. In this case, the sample was raised to 800 °C in an inert atmosphere and held at this temperature for 2 h before cooling down. The figure shows that the sample does not shrink back to its original length at room temperature, but

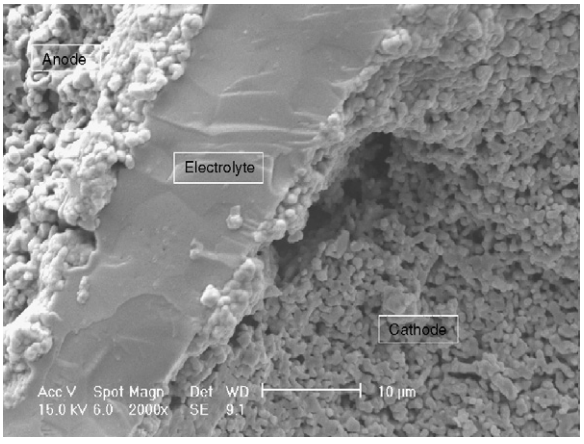

Fig. 13. A micrograph of a typically reduced micro-tubular SOFC.

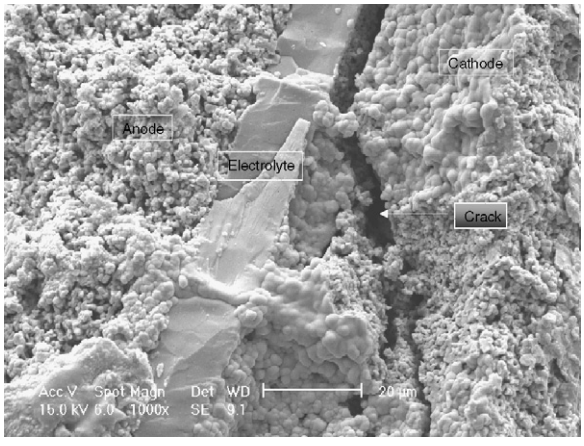

Fig. 15. A micrograph of a micro-tubular SOFC after cycling in 25% excess hydrogen flow.

it remains at $dL/L = 0.1\%$ of its original length. The first derivative of the cycling curve, i.e. $\Delta((dL/L)/dt)$ shows a change of 2 units between the final length and original length, implying that there was bulk volume change in the dimension of the original sample. Irreversible deformation such as this can cause failure in SOFC system. SOFC operated at lower temperatures might be less prone to these irreversible effects. The effect of thermal cycling on the cells was marginal, as no micro-cracks or de-laminations were noticed by SEM.

3.5. SOFC microstructure

Fig. 12 is a cross-sectional scanning electron microscopy (SEM) image of a typically unreduced micro-tubular SOFC. The electrolyte is the dense outer non-porous layer while the anode is the semi-porous layer adhered to the electrolyte. A typical unreduced cell is comprised mainly of NiO/YSZ anode, YSZ electrolyte and LSM cathode. Reduction is carried out using hydrogen, which strips-off the oxygen atom from the Ni particle making the structure more porous, thus enhancing the surface area for fuel oxidation [22] as seen in Fig. 13.

Fig. 14 shows the microstructure of the micro-tubular SOFC cycled in optimum hydrogen flow. No micro-cracking or de-lamination was observed in the micro-structure, suggesting that mere thermal cycling of the tubes might have contributed to stress induction but was not sufficient to cause micro-cracking and de-lamination.

Fig. 15 shows the microstructure of a micro-tubular SOFC cycled in excess hydrogen flow. Small micro-cracks which develop at the material interfaces due to cyclic expansion and contraction during thermal cycling and due to the temperature gradient across the tube are seen to propagate through the electrodes. This is not uncommon in typical SOFC as a small micro-crack can become potential failure zone developing into a large micro-crack, compromising the integrity of the cell and causing failure.

4. Conclusions

The effect of temperature gradients on the isothermal ageing of 25 mm long and 55 mm long microtubes was found to be marginal, as no micro-craking or delamination was observed after post-mortem analysis and SEM. The main cause of degradation during isothermal ageing was Ni particle sintering which changed the microstructure of the micro-tubes and reduces the triple phase boundary layer for fuel oxidation. The trend of degradation during the isothermal ageing with the gradient imposed, closely resembled isothermal ageing without a gradient as reported by Dhir et al. Thus, the temperature gradients imposed might have played a contributive role in the degradation observed but it was not the primary degradation factor.

Thermal cycling on the 55 mm long micro-tube without a temperature gradient, showed no micro-cracking or delamination by SEM, and the initial degradation was dominated by Ni sintering. On the contrary, the micro-tube with the temperature gradient imposed showed both delamination between the electrode–electrolyte layers and micro-cracking. It was adjudged that thermal stress induction due to the CTE mis-match during thermal cycling, together with the diffferential expansion along the tube might have been contributive to the observed degradation.

Also, dilatometry was employed to characterize the sintering effect in micro-tubes. It was found that after each cycle, irreversible deformation occuered in the sample, because the sample failed to recover back to its original length. This irreversible deformation leads to loss of electro-active area necessary for fuel oxidation.

Acknowledgements

We thank Adaptive Materials Inc., USA for supporting this research and the Petroleum Technology Development Fund (PTDF), Nigeria and Univation Ltd., UK for funding also, the Support for one of the co-authors (W. Bujalski within the EU FP6 "RealSOFC" Project, contract no. SES6-CT-3003-502612 is also acknowledged.

References

[1] Y.B. Matus, et al., Solid State Ionics 176 (5–6) (2005) 443–449.
[2] K. Kendall, et al., J. Power Sources 106 (1–2) (2002) 323–327.
[3] M. Liu, et al., J. Power Sources 180 (1) (2008) 215–220.
[4] N. Sakai, et al., Solid State Ionics 177 (19–25) (2006) 1933–1939, Solid State Ionics 15: Proceedings of the 15th International Conference on Solid State Ionics, Part I.
[5] C.M. Dikwal, W. Bujalski, K. Kendall, J. Power Sources 181 (2) (2008) 267–273, Fuel Cells in a Changing World Selected Papers from the Tenth Grove Fuel Cell Symposium.
[6] J. Kong, et al., Rare Metals 25 (6, Supplement 1) (2006) 300–304.
[7] D. Waldbillig, A. Wood, D.G. Ivey, J. Power Sources 145 (2) (2005) 206–215, Selected papers presented at the Fuel Cells Science and Technology Meeting.
[8] D. Waldbillig, A. Wood, D.G. Ivey, Solid State Ionics 176 (9–10) (2005) 847–859.
[9] M.-F. Han, et al., Solid State Ionics 179 (27–32) (2008) 1545–1548, Solid State Ionics 16: Proceedings of the 16th International Conference on Solid State Ionics (SSI-16), Part II.
[10] S.-D. Kim, et al., Solid State Ionics 177 (9–10) (2006) 931–938.
[11] L. Zhou, et al., Electrochim. Acta 53 (16) (2008) 5195–5198.
[12] K. Nikooyeh, A.A. Jeje, J.M. Hill, J. Power Sources 171 (2) (2007) 601–609.
[13] A. Nakajo, et al., J. Power Sources 158 (1) (2006) 287–294.
[14] W. Bujalski, et al., J. Power Sources 157 (2) (2006) 745–749, Selected papers presented at the Ninth Grove Fuel Cell Symposium.
[15] C. Mallon, K. Kendall, J. Power Sources 145 (2) (2005) 154–160, Selected papers presented at the Fuel Cells Science and Technology Meeting.
[16] A. Dhir, K. Kendall, J. Power Sources 181 (2) (2008) 297–303, Fuel Cells in a Changing World Selected Papers from the Tenth Grove Fuel Cell Symposium.
[17] W. Bujalski, C.M. Dikwal, K. Kendall, J. Power Sources 171 (1) (2007) 96–100, Scientific Advances in Fuel Cell Systems, Turin, Italy, 13–14 September 2006.
[18] B.D. Madsen, S.A. Barnett, Solid State Ionics 176 (35–36) (2005) 2545–2553.
[19] J.I. Gazzarri, O. Kesler, J. Power Sources 167 (2) (2007) 430–441.
[20] Y.-S. Chou, J.W. Stevenson, J. Power Sources 140 (2) (2005) 340–345.
[21] J.L.a.A. Dicks, Fuel Cells Systems Explained, 2nd ed., 2003.
[22] D. Sarantaridis, R.A. Rudkin, A. Atkinson, J. Power Sources 180 (2) (2008) 704–710.